

Article

# Theoretical Study on the Hydrogenation Mechanisms of Model Compounds of Heavy Oil in a Plasma-Driven Catalytic System

Haigang Hao <sup>1,†</sup>, Pengfei Lian <sup>2,†</sup>, Juhui Gong <sup>1</sup> and Rui Gao <sup>1,\*</sup>

<sup>1</sup> College of Chemistry and Chemical Engineering, Inner Mongolia University, Hohhot 010021, China; haohaigang@imu.edu.cn (H.H.); imugongjuhui@163.com (J.G.)

<sup>2</sup> University of Chinese Academy of Sciences, Beijing 100049, China; lianpengfei1985@163.com

\* Correspondence: gaorui@imu.edu.cn; Tel.: +86-0471-4995-400

† These authors contributed equally to this work.

Received: 6 August 2018; Accepted: 3 September 2018; Published: 7 September 2018



**Abstract:** Heavy oil will likely dominate the future energy market. Nevertheless, processing heavy oils using conventional technologies has to face the problems of high hydrogen partial pressure and catalyst deactivation. Our previous work reported a novel method to upgrade heavy oil using hydrogen non-thermal plasma under atmospheric pressure without a catalyst. However, the plasma-driven catalytic hydrogenation mechanism is still ambiguous. In this work, we investigated the intrinsic mechanism of hydrogenating heavy oil in a plasma-driven catalytic system based on density functional theory (DFT) calculations. Two model compounds, toluene and 4-ethyltoluene have been chosen to represent heavy oil, respectively; a hydrogen atom and ethyl radical have been chosen to represent the high reactivity species generated by plasma, respectively. DFT study results indicate that toluene is easily hydrogenated by hydrogen atoms, but hard to hydrocrack into benzene and methane; small radicals, like ethyl radicals, are prone to attach to the carbon atoms in aromatic rings, which is interpreted as the reason for the increased substitution index of trap oil. The present work investigated the hydrogenation mechanism of heavy oil in a plasma-driven catalytic system, both thermodynamically and kinetically.

**Keywords:** heavy oil; plasma; catalytic mechanism; hydrogenation; hydrocracking; DFT calculation

## 1. Introduction

Heavy oil, including heavy, extra heavy crude and refinery residue, will likely dominate the future energy market because high-quality light crude is becoming depleted and more expensive. Nevertheless, heavy oil has a low H/C atomic ratio and a high content of heteroatoms (e.g., nitrogen, sulfur and trace metals) compared to light crude [1], which is a challenge for processing heavy oils using conventional technologies.

Carbon rejection and hydrogenation are two general routes for upgrading heavy oil [2]. Carbon rejection processes extract the light products from heavy oil by thermal cracking, which usually leads to the quality of light products being poor. The hydrogenation process could suppress coke formation and improve the quality of light products, with the aid of a catalyst under a high hydrogen partial pressure [3,4]. However, the hydrogenation process has to face two problems: (1) The high cost of operating and reactor manufacturing due to high hydrogen partial pressure and (2) catalyst deactivation because of carbon and metal deposition on the catalyst surface [5,6]. Therefore, developing a novel technology to decrease high hydrogen partial pressure and solve the problem of catalyst deactivation is necessary.

Our previous work [7] reported a novel method to upgrade heavy oil using hydrogen non-thermal plasma under atmospheric pressure without a catalyst. Plasma is an electroneutral mixture and contains electroneutral gas molecules, as well as electrons, ions, atoms, radicals, photons and excited molecules, which are chemically and physically active species [8]. Due to the high reactivity, plasma has been used in many fields, such as gas cleaning, surface treatment and ozone production [9–18].

In our previous work [7], although it has been demonstrated that non-thermal plasma could increase light oil yield significantly and add hydrogen to heavy oil under atmospheric pressure without a catalyst, the plasma-driven catalytic hydrogenation mechanism is still ambiguous, especially the reason for the increased substitution index of trap oil.

The density functional theory (DFT) has been used to study the thermodynamics associated with steam reforming of small organic molecules (e.g., DiMethyl Ether and Ethanol) under cold plasma conditions [19,20]. These studies focused on the dissociation of original reactants forming radicals through the highly energetic electrons within cold plasmas and the following radical reactions. The calculation results showed that the thermodynamic obstacle was easy to be overcome under cold plasma conditions. A DFT study has also been used to study the interaction of plasma species with the catalyst surface to reveal the effect of plasma and explain the reaction mechanism under plasma conditions [21–23].

The hydrogenation mechanisms of heavy oil on traditional catalysts were also widely investigated using DFT [24–26]. Due to the complex of reaction and reactants, model compounds, such as thiophene pyridine, 2,6-dimethylpyridine and benzyl radical, were selected to represent the heavy oil.

Thus, there is a lack of theoretical studies about the hydrogenation mechanism of heavy oil in a plasma-driven catalytic system. This study attempts to reveal the plasma-driven catalytic hydrogenating mechanism of heavy oil using DFT calculation. Toluene and 4-ethyltoluene have been chosen as the heavy oil model compounds, respectively; a hydrogen atom and ethyl radical have been chosen as the high reactivity species generated in a plasma-driven catalytic reaction system.

DFT study results indicate that toluene is easily hydrogenated by hydrogen atoms, but hard to hydrocrack into benzene and methane. Furthermore, it also shows that small radicals, like ethyl radicals, are prone to attach to the carbon atoms in the 4-ethyltoluene ring, which is interpreted as the reason for the increased substitution index of trap oil.

## 2. Results

Heavy oils mainly consist of aromatic-kind compounds, which account for more than 70% [7]. Most heavy oil molecules are condensed aromatic rings (with side chains) connected by bridge bonds [1]. Heavy oils crack into small pieces under reaction conditions and the final products depend on the type of fragments generated. According to the structure and composition of heavy oil, model compounds of which has been represented by toluene and 4-ethyltoluene, respectively.

Plasma is an ionized gas which is generated by heating a gas to a high temperature or by applying a strong electromagnetic field (or a high voltage electrical field) to a gas. Therefore, all kinds of gases in a plasma system would be partially ionized into a plasma state. Gases, such as methane and ethane, generated by the thermal cracking of heavy oil would be partially ionized into a plasma state inevitably and some of them would become small radicals (e.g., methyl and ethyl). Hence, hydrogen atoms and ethyl radicals have been chosen to represent the high reactivity species in our plasma-driven catalytic system.

According to the selected reactants, two categories of reaction were designed to illuminate the plasma-driven catalytic hydrogenation mechanisms: (1) Hydrogen atoms reacted with toluene and (2) the ethyl radical reacted with 4-ethyltoluene.

## 2.1. Hydrogen Atom Reacted with Toluene

To clearly understand and describe the hydrogenation/hydrocracking pathways of toluene, the seven carbon atoms of toluene are labeled as C<sub>1</sub>–C<sub>7</sub> (see Figure 1). Clearly, it can be seen that C<sub>2</sub> is equivalent to C<sub>6</sub>, and C<sub>3</sub> is equivalent to C<sub>5</sub>.

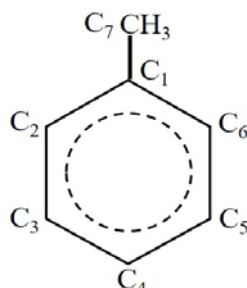


**Figure 1.** The naming rule for carbon atoms in toluene for this study.

Firstly, all the reaction routes of hydrogenating toluene (namely the original reactant) by the first hydrogen atom have been calculated. In Figure 2a, the DFT results demonstrate that a hydrogen atom is most easily added to C<sub>2</sub> (or C<sub>6</sub>) of toluene with the lowest barrier of 10.5 kJ/mol, and its reaction energy is –115.5 kJ/mol (blue line); while, hydrogenating C<sub>1</sub> has the highest barrier of 18.4 kJ/mol, and its reaction energy is –99.8 kJ/mol (pink line).

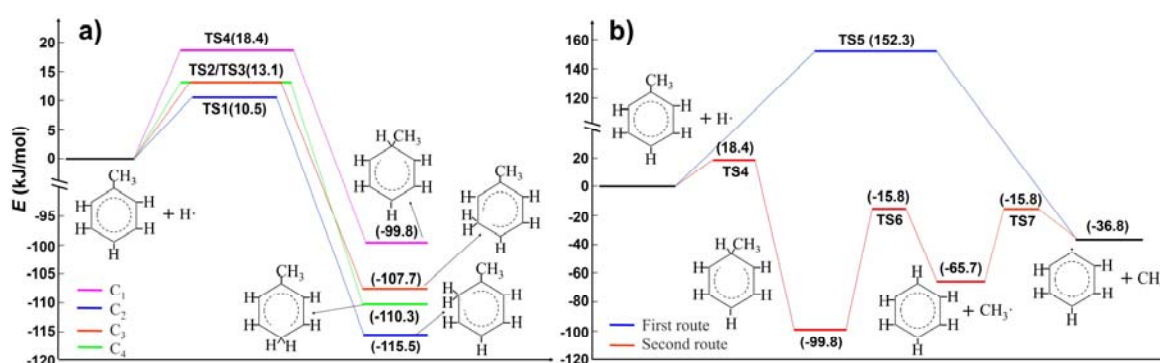


**Figure 2.** The energy profiles: (a) Hydrogenation of toluene (the original reactant) by the first hydrogen atom; (b) hydrocracking of toluene (the original reactant) by the first hydrogen atom.

In Figure 2b, two reaction routes of hydrocracking toluene into benzene and methane were calculated. In the first route (blue line), C<sub>7</sub> was directly attacked by the H atom to generate a phenyl group and methane, which was exothermic by 36.8 kJ/mol, with a very high barrier of 152.3 kJ/mol. In the second route (red line), C<sub>1</sub> was attacked by the H atom producing a phenyl group and methane. For the first step of the second route, the H atom is easily added to C<sub>1</sub> forming C<sub>6</sub>H<sub>6</sub>CH<sub>3</sub> (first-generation hydrogenated products), its energy barrier is only 18.4 kJ/mol. However, the consequent cracking of C<sub>6</sub>H<sub>6</sub>CH<sub>3</sub> into benzene and methyl is difficult, which needs a higher energy barrier of 84.0 kJ/mol, and is an endothermic reaction (34.1 kJ/mol). After that, although the methyl captures the H atom of benzene, forming a phenyl group and methane with a lower barrier of 49.9 kJ/mol and an endothermic energy of 28.9 kJ/mol, it is reasonably inferred that this step is less likely, because the methyl is prone to capture the hydrogen atom generated by plasma in the atmosphere with a limited barrier. Totally, the calculation results indicate that the hydrogenation probability of toluene is higher than that of hydrocracking toluene, both thermodynamically (–115.5 vs. –36.8 kJ/mol) and kinetically (10.5 vs. 84.0 kJ/mol).

According to the above calculations of toluene hydrogenation by the first H atom, the further hydrogenation of C<sub>6</sub>H<sub>6</sub>CH<sub>3</sub> (first-generation hydrogenated product) into C<sub>6</sub>H<sub>7</sub>CH<sub>3</sub> (second-generation

hydrogenated product) by the second H atom was investigated in Figure 3. Here, it must be pointed out that the first H atom is added on the C<sub>2</sub> site of toluene, forming C<sub>6</sub>H<sub>6</sub>CH<sub>3</sub> (first-generation hydrogenated product). In Figure 3, the DFT calculation results show that, except for C<sub>5</sub> (red dash line, energy barrier is 97.1 kJ/mol), the other four carbon sites (C<sub>3</sub>, C<sub>4</sub>, C<sub>6</sub> and C<sub>1</sub>) of C<sub>6</sub>H<sub>6</sub>CH<sub>3</sub> (first-generation hydrogenated product) were easily hydrogenated by the second H atom with barriers lower than 40 kJ/mol. However, the hydrogenation of C<sub>3</sub> (red line) and C<sub>1</sub> (pink line) sites of first-generation hydrogenated products are more favorable (−322.9 and −307.2 kJ/mol) thermodynamically, suggesting the C–C single bonds are easily formed in the aromatic ring.

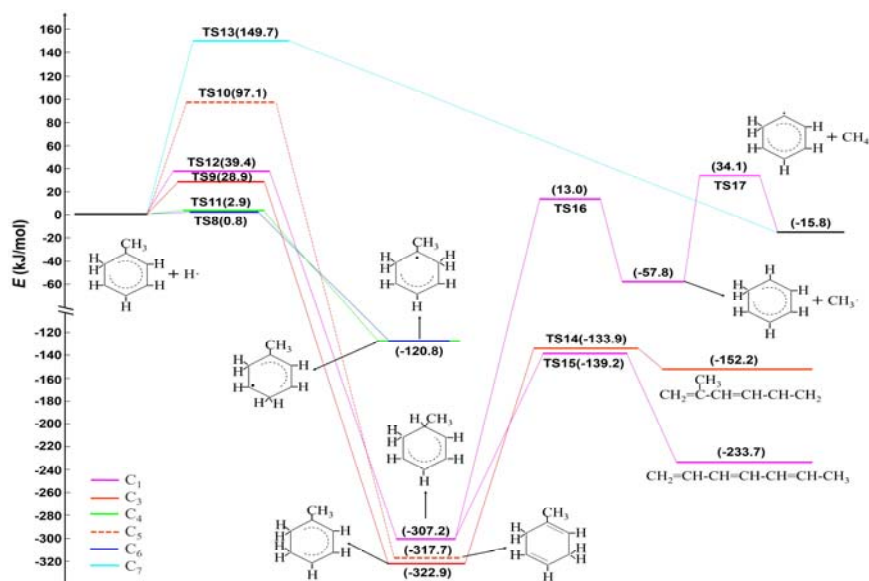


**Figure 3.** Energy profiles of hydrogenation and hydrocracking by the second H atom for first-generation hydrogenated products.

Consequently, in Figure 3, the breaking of one of these two C–C single bonds (C<sub>1</sub>–C<sub>2</sub> and C<sub>2</sub>–C<sub>3</sub>) of C<sub>6</sub>H<sub>7</sub>CH<sub>3</sub> (second-generation hydrogenated product), as well as the hydrocracking of the single bond (C<sub>1</sub>–C<sub>7</sub>) by the second H atom were calculated as well. Compared with the hydrogenations, cracking single bonds (TS14–TS17) are endothermic reactions, their effective barriers are higher than 168 kJ/mol. The hydrocracking C<sub>1</sub>–C<sub>7</sub> single bond of C<sub>6</sub>H<sub>7</sub>CH<sub>3</sub> into benzene and methane (TS13) is an exothermic reaction (−15.8 kJ/mol) but with a high barrier of 149.7 kJ/mol as well.

Similarly, the calculations of hydrogenation and hydrocracking by the third H atom for second-generation hydrogenated products have also been carried out as displayed in Figure 4. According to the above calculations, it must be declared that the first two H atoms were added to the C<sub>2</sub> and C<sub>3</sub> sites of toluene. Compared with the previous hydrogenation reaction, the energy barriers decreased for the hydrogenation of the second-generation hydrogenated product by the third H atom. The hydrogenating C<sub>4</sub> of the second-generation hydrogenated product by the third H atom is even without barriers. Compared with hydrogenation, the hydrocracking of the single bond in second-generation hydrogenated products is still difficult and needs high barriers (the effective barriers are higher than 156 kJ/mol).

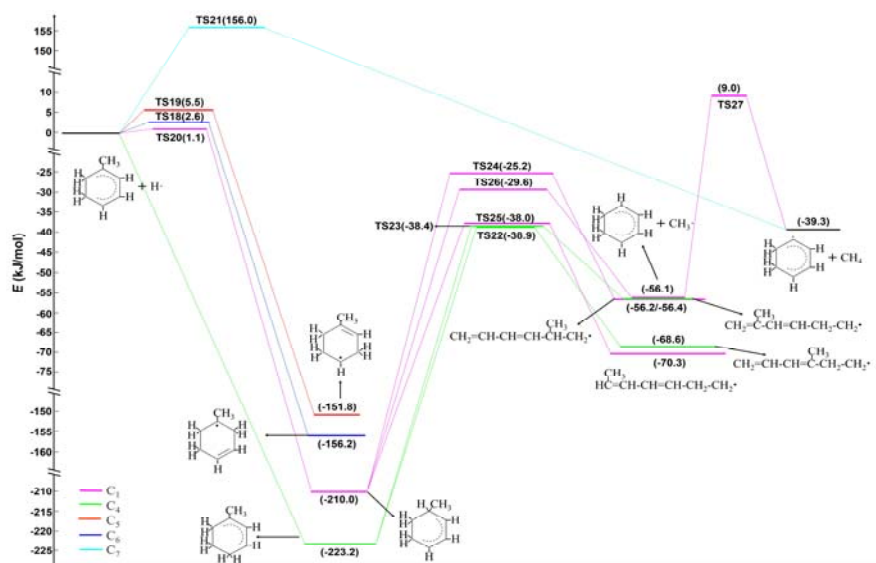


**Figure 4.** Energy profiles of hydrogenation and hydrocracking by the third H atom for second-generation hydrogenated products.

Further calculations (see Supplementary Materials) proved that the fourth, fifth and sixth H atom generated by non-thermal plasma could easily be added into the aromatic ring, both thermodynamically and kinetically. A reaction scheme along with the reaction energy of the toluene hydrogenating sequence is given in Figure 5 which can be very helpful to understand the toluene hydrogenation processes.

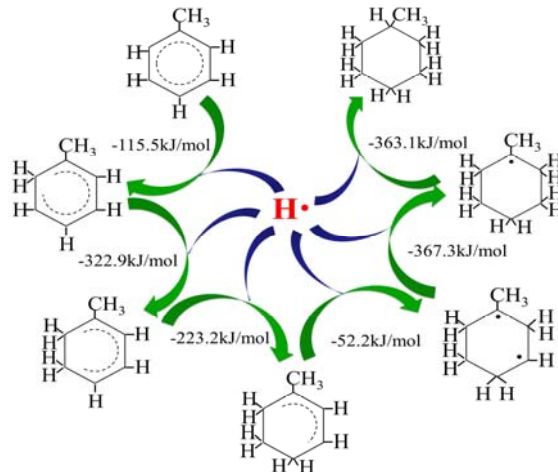


**Figure 5.** Reaction scheme of the toluene hydrogenation process.

Via the aforementioned theoretical studies, as well as our previous experimental results, it is reasonably speculated that the H atoms generated by non-thermal plasma could easily be continuously added into aromatic rings, but hydrocracking the aromatic rings of heavy oil is difficult both thermodynamically and kinetically. The results of this DFT calculation well explained the hydrogenation mechanism of heavy oil under a hydrogen plasma condition.

## 2.2. Ethyl Radical Reacted with 4-Ethyltoluene

As mentioned before, gases, such as methane and ethane, generated by thermal cracking of heavy oil, would be partially ionized into a plasma state (small radicals, like methyl and ethyl) inevitably. Therefore, ethyl radical was chosen as the high reactivity species of plasma in this section, to react with

the heavy oil model compound of 4-ethyltoluene. In Figure 6, eight reaction routes were designed to disclose the intrinsic mechanism of the plasma-driven catalytic hydrogenation of heavy oil. These eight designed reaction routes were divided into two categories: (1) The ethyl radical reacted with the side chain (e.g.,  $-\text{CH}_3$  or  $-\text{C}_2\text{H}_5$ ) of the benzene ring; and (2) the ethyl radical reacted with the carbon atoms of the benzene ring.

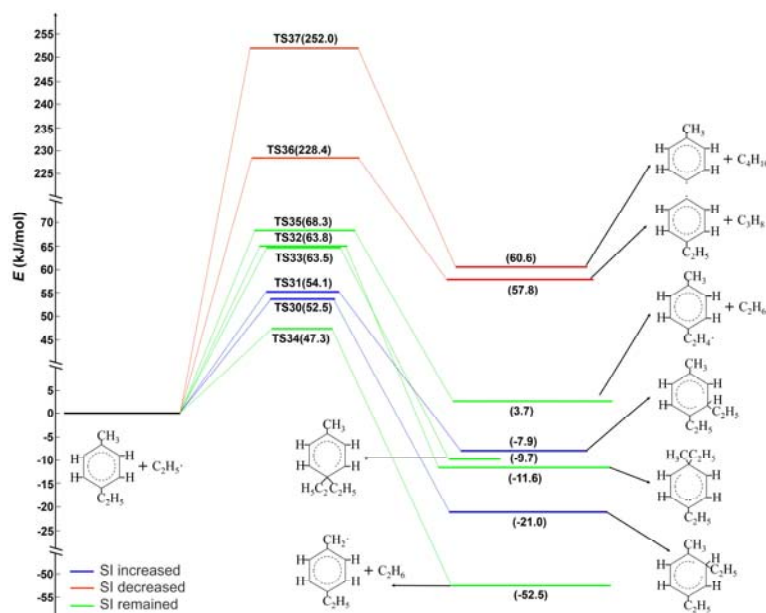


**Figure 6.** Energy profiles of the ethyl radical reacted with 4-ethyltoluene (SI: Substitution Index).

For the former, the ethyl radical either directly attacks the hydrogen atoms of the side chain or attacks the carbon atoms of the side chain. In Figure 6, DFT calculations show that the ethyl radical is prone to capture the hydrogen at the end position of the side chain in 4-ethyltoluene (barriers  $< 70$  kJ/mol) rather than attack the carbon atoms of the side chain forming into a bigger alkane and a smaller alkyl-benzene (barrier  $> 220$  kJ/mol). With regard to the later, the calculation results indicate that the ethyl radical attacking the carbon atom of the benzene ring in 4-ethyltoluene is exothermic and the barriers are between 52.5 and 63.8 kJ/mol.

Totally, for comparison, the ethyl radical favorably attacks the carbon atoms of the benzene ring or the hydrogen atoms at the end position of the side chain both thermodynamically and kinetically. In other words, the small radicals would increase (blue line) or sustain (green line) the substitution index of the aromatic ring, but have difficulty decreasing (red line) the substitution index of the aromatic ring, which is well in agreement with our previous work [7].

### 3. Discussion

In summary, the calculations in this study demonstrate that the benzene ring of toluene is easily hydrogenated by H atoms generated by plasma with a lower barrier, while the side chain of aromatic rings is hardly hydrocracked by the high reactivity species (e.g., the H atom and ethyl radical). That is to say, our study indicates that it is not feasible to process heavy oil by non-thermal plasma alone, because non-thermal plasma does not have enough energy to crack the C–C bonds of heavy oil molecules. In our previous work [7], it has been proved that heavy oil can be upgraded only when non-thermal plasma is coupled with traditional thermal cracking; in which the non-thermal plasma technology mainly provides the high reactivity species, while the thermal cracking technology primarily provides the energy to break C–C bonds in heavy oil molecules.

It has been reported that methane, ethane and even butane would be partially ionized into plasma state (methyl, ethyl and butyl) in the plasma-driven catalytic system in our former study. These high

reactivity radicals can promptly react with the aromatic rings of trap oil (gas state under reaction conditions), which finally increase the substitution index of trap oil. In this work, the calculations clearly disclose that small radicals are prone to increase the substitution index rather than decrease the substitution index of aromatic rings, which explains our experimental phenomenon.

In the future, other high reactivity species (such as ions, excited molecules and even free electrons) should be studied to discover the role of these reactivity species and the corresponding intrinsic hydrogenation mechanism of heavy oil in a plasma-driven catalytic system.

#### 4. Materials and Methods

All calculations were performed using Gaussian 09 program package [27]. The geometry of each compound and the radical structure were optimized using the DFT method with B3LYP/6-311+G(d,p) basis set was performed [28–30]. All Cartesian coordinates of the intervening species have been given in Supplementary Materials. Except for the stable structures without single electron spin, all other optimized structures are calculated used the unrestricted wave function. Frequency calculations were carried out to check whether each stationary was an intermediate (no negative frequency) or a transition state (exactly only one negative frequency, see Supplementary Materials). Furthermore, for some suspicious transition states, the intrinsic reaction coordinate (IRC) calculations [31] were performed for both forward and reverse directions to confirm that the optimized transition states correctly connect the relevant reactants and products. For the reactions, the relative energy ( $\Delta E$ ), enthalpy ( $\Delta H$ ) and Gibbs free energy ( $\Delta G$ ) are calculated at 298.15 K.

The barrier ( $E_a$ ) and reaction energy ( $\Delta G$ ) were calculated according to  $E_a = E_{TS} - E_{IS}$  and  $\Delta G = E_{FS} - E_{IS}$ , where  $E_{IS}$ ,  $E_{FS}$  and  $E_{TS}$  are the sum of electronic and thermal free energies of the corresponding initial state (IS), final state (FS) and transition state (TS), respectively.

**Supplementary Materials:** The following are available online at <http://www.mdpi.com/2073-4344/8/9/381/s1>, Figure S1. Energy profiles of hydrogenation and hydrocracking by the fourth H atom for third-generation hydrogenated products, Figure S2. Energy profiles of hydrogenation by the fifth H atom (a) and sixth H atom (b) for fourth-generation and fifth-generation hydrogenated products, Figure S3. The structures of transition states for the model compound hydrogenation in the energy profiles, Table S1. The bond length of transition states for the model compound hydrogenation in the energy profiles, Table S2. The Cartesian coordinates of intervening species (reactants, transition states and products) in the energy profiles.

**Author Contributions:** Performing the first part calculations, analyzing the data and writing the original draft preparation, H.H.; performing the second part calculations and analyzing the data, P.L.; analyzing the data and plotting the figures of the article, J.G.; project supervision and writing review, R.G.

**Funding:** This research was funded by the Program of Higher-level Talents of IMU (21300-5185111) and Program of Higher-level Talents of IMU (21300-5185109).

**Acknowledgments:** The authors are grateful for advice from Jianli Yang. We also acknowledge Synfuels China, Co. Ltd. for the free use of their Super-Server for the DFT calculations.

**Conflicts of Interest:** The authors declare no conflicts of interest.

#### References

1. Rana, M.S.; Samano, V.; Ancheyta, J.; Diaz, J.A.I. A review of recent advances on process technologies for upgrading of heavy oils and residua. *Fuel* **2007**, *86*, 1216–1231. [CrossRef]
2. Speight, J.G. New approaches to hydroprocessing. *Catal. Today* **2004**, *98*, 55–60. [CrossRef]
3. Zhang, S.; Liu, D.; Deng, W.; Que, G. A review of slurry-phase hydrocracking heavy oil technology. *Energy Fuels* **2007**, *21*, 3057–3062. [CrossRef]
4. Furimsky, E. Selection of catalysts and reactors for hydroprocessing. *Appl. Catal. A* **1998**, *171*, 177–206. [CrossRef]
5. Zhang, X.; Chodakowski, M.; Shaw, J.M. Impact of multiphase behavior on coke deposition in a commercial hydrotreating catalyst under sedimentation conditions. *Energy Fuels* **2005**, *19*, 1405–1411. [CrossRef]

6. Yang, M.G.; Nakamura, I.; Fujimoto, K. Hydro-thermal cracking of heavy oils and its model compound. *Catal. Today* **1998**, *43*, 273–280. [[CrossRef](#)]
7. Hao, H.G.; Wu, B.S.; Yang, J.L.; Guo, Q.; Yang, Y.; Li, Y.W. Non-thermal plasma enhanced heavy oil upgrading. *Fuel* **2015**, *149*, 162–173. [[CrossRef](#)]
8. Tendero, C.; Tixier, C.; Tristant, P.; Desmaison, J.; Leprince, P. Atmospheric pressure plasmas: A review. *Spectrochim. Acta Part B* **2006**, *61*, 2–30. [[CrossRef](#)]
9. Van Durme, J.; Dewulf, J.; Leys, C.; Van Langenhove, H. Combining non-thermal plasma with heterogeneous catalysis in waste gas treatment: A review. *Appl. Catal. B* **2008**, *78*, 324–333. [[CrossRef](#)]
10. Kogelschatz, U. Dielectric-barrier discharges: Their history, discharge physics, and industrial applications. *Plasma Chem. Plasma Process.* **2003**, *23*, 1–46. [[CrossRef](#)]
11. Chirokov, A.; Gutsol, A.; Fridman, A. Atmospheric pressure plasma of dielectric barrier discharges. *Pure Appl. Chem.* **2005**, *77*, 487–495. [[CrossRef](#)]
12. Rollier, J.D.; Gonzalez-Aguilar, J.; Petitpas, G.; Darmon, A.; Fulcheri, L.; Metkemeijer, R. Experimental study on gasoline reforming assisted by nonthermal arc discharge. *Energy Fuels* **2008**, *22*, 556–560. [[CrossRef](#)]
13. Eliasson, B.; Liu, C.J.; Kogelschatz, U. Direct conversion of methane and carbon dioxide to higher hydrocarbons using catalytic dielectric-barrier discharges with zeolites. *Ind. Eng. Chem. Res.* **2000**, *39*, 1221–1227. [[CrossRef](#)]
14. Li, M.W.; Tian, Y.L.; Xu, G.H. Characteristics of carbon dioxide reforming of methane via alternating current (AC) corona plasma reactions. *Energy Fuels* **2007**, *21*, 2335–2339. [[CrossRef](#)]
15. Matsui, Y.; Kawakami, S.; Takashima, K.; Katsura, S.; Mizuno, A. Liquid-phase fuel reforming at room temperature using non-thermal plasma. *Energy Fuels* **2005**, *19*, 1561–1565. [[CrossRef](#)]
16. Veerapandian, S.K.; Leys, C.; De Geyter, N.; Morent, R. Abatement of VOCs using packed bed non-thermal plasma reactors: A review. *Catalysts* **2017**, *7*, 113. [[CrossRef](#)]
17. Yap, D.; Tatibouët, J.M.; Batiot-Dupeyrat, C. Catalyst assisted by non-thermal plasma in dry reforming of methane at low temperature. *Catal. Today* **2018**, *299*, 263–271. [[CrossRef](#)]
18. Ma, S.; Zhao, Y.; Yang, J.; Zhang, S.; Zhang, J.; Zheng, C. Research progress of pollutants removal from coal-fired flue gas using non-thermal plasma. *Renew. Sustain. Energy Rev.* **2017**, *67*, 791–810. [[CrossRef](#)]
19. Pan, Y.X.; Han, Y.; Liu, C.J. Pathways for steam reforming of dimethyl ether under cold plasma conditions: A DFT study. *Fuel* **2007**, *86*, 2300–2307. [[CrossRef](#)]
20. Wang, W.; Zhu, C.; Cao, Y. DFT study on pathways of steam reforming of ethanol under cold plasma conditions for hydrogen generation. *Int. J. Hydrogen Energy* **2010**, *35*, 1951–1956. [[CrossRef](#)]
21. Mistry, H.; Choi, Y.W.; Bagger, A.; Scholten, F.; Bonifacio, C.; Sinev, I.; Stach, E.A. Enhanced carbon dioxide electroreduction to carbon monoxide over defect rich plasma-activated silver catalysts. *Angew. Chem.* **2017**, *129*, 11552–11556. [[CrossRef](#)]
22. Shirazi, M.; Neyts, E.C.; Bogaerts, A. DFT study of Ni-catalyzed plasma dry reforming of methane. *Appl. Catal. B* **2017**, *205*, 605–614. [[CrossRef](#)]
23. Somers, W.; Bogaerts, A.; van Duin, A.C.T.; Neyts, E.C. Plasma species interacting with nickel surfaces: Toward an atomic scale understanding of plasma-catalysis. *J. Phys. Chem. C* **2012**, *116*, 20958–20965. [[CrossRef](#)]
24. Stoyanov, S.R.; Gusarov, S.; Kuznicki, S.M.; Kovalenko, A. Theoretical modeling of zeolite nanoparticle surface acidity for heavy oil upgrading. *J. Phys. Chem. C* **2008**, *112*, 6794–6810. [[CrossRef](#)]
25. Ding, S.; Jiang, S.; Zhou, Y.; Wei, Q.; Zhou, W. Oxygen effects on the structure and hydrogenation activity of the MoS<sub>2</sub> active site: A mechanism study by DFT calculation. *Fuel* **2017**, *194*, 63–74. [[CrossRef](#)]
26. Hou, P.; Zhou, Y.; Guo, W.; Ren, P.; Guo, Q.; Xiang, H.; Yang, Y. Rational design of hydrogen-donor solvents for direct coal liquefaction. *Energy Fuels* **2018**, *32*, 4715–4723. [[CrossRef](#)]
27. Frisch, M.J.; Trucks, G.W.; Schlegel, H.B.; Scuseria, G.E.; Robb, M.A.; Cheeseman, J.R.; Scalmani, G.; Barone, V.; Mennucci, B.; Petersson, G.A.; et al. *Gaussian 09, Revision, A. 02*; Gaussian, Inc.: Wallingford, CT, USA, 2009.
28. Becke, A.D. Density-functional thermochemistry. III. The role of exact exchange. *J. Chem. Phys.* **1993**, *98*, 5648–5652. [[CrossRef](#)]
29. Becke, A.D. Density-functional exchange-energy approximation with correct asymptotic behavior. *Phys. Rev. A* **1988**, *38*, 3098–3100. [[CrossRef](#)]

30. Lee, C.; Yang, W.; Parr, R.G. Development of the Colle-Salvetti correlation-energy formula into a functional of the electron density. *Phys. Rev. B* **1988**, *37*, 785–789. [[CrossRef](#)]
31. Gonzalez, C.; Schlegel, H.B. An improved algorithm for reaction path following. *J. Chem. Phys.* **1989**, *90*, 2154–2161. [[CrossRef](#)]



© 2018 by the authors. Licensee MDPI, Basel, Switzerland. This article is an open access article distributed under the terms and conditions of the Creative Commons Attribution (CC BY) license (<http://creativecommons.org/licenses/by/4.0/>).